Influence of Intermolecular Interactions in the Redox Performance of Surface Confined Probes. Kinetic Measurements with Square Wave Voltammetry: Beyond the Quasi-Reversible Maximum

Joaquin Gonzalez*, Jose-Alfonso Sequí

Departamento de Química Física, Facultad de Química, Regional Campus of International Excellence "Campus Mare Nostrum", Universidad de Murcia, 30100 Murcia, Spain

Corresponding author

* E-mail: josquin@um.es

ORCID

Joaquin Gonzalez: 0000-0001-6848-074X

Abstract

Analysis of the Square Wave Voltammetry (SWV) responses of surface confined electroactive probes under finite kinetics conditions, by considering the influence of intermolecular interactions on the current, is presented. This non-ideality gives rise to very significant deviations in the most relevant features of the current potential response as compared with predictions of ideal models. The theoretical model does not require that the dependence of the rate constant with the potential (i. e., Butler-Volmer or Marcus-Hush kinetic formalisms) is explicitly established a priori. Both location and height of the Quasi-Reversible Maximum and symmetry of the SWV current-potential curves are strongly affected by the interaction parameters $G = a_{OO} + a_{RR} - 2a_{OR}$ and $S = a_{RR} - a_{OO}$ (with a_{ij} being the interaction coefficient for species i and j). Quantitative methods for obtaining kinetic and interaction parameters of the redox probes are presented, based on the measurement of the peak currents and potential under quasi-reversible conditions where the current exhibits two asymmetric peaks. A discussion is done concerning the deviations found in the estimation of the rate constants with SWV when intermolecular interactions are not considered. The above methods have been applied to the characterisation of mixed ferrocenylundecanethiol / decanethiol monolayers on gold electrodes at an ethanolic medium for which the SWV is clearly non-ideal.

Keywords

Square Wave Voltammetry, Electroactive Monolayer, Intermolecular Interactions, Electrode kinetics, Marcus-Hush formalism, Butler-Volmer formalism

1. Introduction

The tailored design of electrochemical interfaces or devices based on surface confined electroactive molecules for an specific purpose is strongly conditioned by their redox functionality. Among the different applications of these systems are, for example, their use on molecular electronics, electrocatalysis-based devices, electrochemical synthesis processes, etc., [1-10]. This redox functionality is based on a sequence of relevant charge transfer processes and is determined by, among other factors, the value of the electrochemical rate constant of the same, which can be strongly influenced by the medium in which it takes place. In the case of confined redox probes, the interfacial environment of the electroactive groups is critical for its redox performance [11-17].

There exists a variety of different electrochemical methods for the measurement of the electrochemical rate constant and other related variables. The method most frequently employed is Cyclic Voltammetry, for which, based on Laviron's ideal model, the rate constant is obtained from the shift of the voltammetric peak potentials in terms of the scan rate [11, 12, 18]. This methodology, although broadly used, present several limitations. Thus, it needs the a priori assumption of a given kinetic formalism, typically the Butler-Volmer (BV) one. Moreover, it does not consider the influences of non-idealities. Also, under BV conditions, the charge transfer coefficient needs to be determined in order to know the electrochemical rate constant [18-20]. Other useful approaches are those based on the use of alternating current measurements as Alternating Current Voltammetry (ACS) and Electrochemical Impedance Spectroscopy (EIS) [18, 21], which also relies on the consideration of "external" models, in this case, the suitability of a given equivalent circuit, which can be very complex, to the experimental data. Among ACS methods, those based on the Fourier transformation of large amplitude ACS are of great interest since it is possible to analyse a great amount of data arising from different harmonics. This has allowed its application to a great number of experimental situations [22-25]. Nevertheless, the theoretical treatment of these responses is complex and, in the case of surface confined electroactive systems, mostly ideal responses have been addressed.

An interesting alternative to the above methods are the potential pulse techniques in which the current arising from the application of a given potential pulse sequence is measured versus time (cronoamperometric methods) [17, 20, 26], or at a given time in terms of the applied potential (voltammetric techniques) [20, 27-31]. These methods have several advantages as the de-coupling of double layer and faradaic contributions to the overall current, they do not require any a priori assumptions in the kinetic formalism, and they present an enhanced sensitivity arising from the sample procedure of the current [20, 26, 32]. Among the potential pulse techniques, Square Wave Voltammetry presents a special interest. It was introduced by Baker [33] and extensively developed by Osteryoung and co-workers, and Lovric and co-workers [27-30, 34-36]. Hence, like scanning methods, SWV is a fast technique since a square wave voltammogram can be obtained

over a wide potential range in a matter of seconds and can therefore be used in combination with other analytical methods such are, for example, chromatographic techniques. SWV, like differential pulse techniques, it is a purely subtractive technique, and therefore the non faradaic and background currents are minimized. The most significant, differentiating characteristic of SWV lies in the use of repeated oxidation and reduction of analyte species, which means that sensitivity is enhanced and kinetic information is provided, because of the ability to analyse both the forward and the reverse currents, as well as the net current. Thus, information about the reaction reversibility can be obtained easily. In the case of surface confined molecules, Lovric et al proposed to determine the electrochemical rate constant from the so-called Quasi-Reversible Maximum (QRM), that is, the maximum peak current obtained in terms of the frequency of the potential perturbation, which corresponds to a typical quasi-reversible behaviour [27, 29, 37, 38]. Alternatively, Mirceski proposed a similar approach based on the influence of the square wave amplitude for a fixed frequency [39].

Potential pulse methods, and SWV in particular, should provide very accurate values of electrochemical rate constants. However, as in the previous cases, the different approaches for the modelling of the electron transfer behaviour of surface confined redox probes are mostly based on simple models that only consider idealized probe-surface interactions, and lead to simplistic cartoons of the experimental responses [17, 40]. A first approach to achieve a more accurate description of the electrochemical behaviour of modified interfaces is to consider the existence of intermolecular interactions, which can be, in general, of repulsive or attractive nature. The causes of these interactions are related with the appearance of coulombic long range repulsions, or with the presence of attractive Van der Waals interactions (i. e., odd-even) or π-π interactions, among others [13-15, 17]. The influence of interactions in the electrochemical response of the surface redox probes is quantized through potential-independent interaction parameters *G* and *S*, introduced by Laviron, among other authors, when considering a Frumkin type of adsorption isotherm [12, 17, 41]. In the case of SWV, as far as we know, only a previous reference by Lovric et al has included the consideration of intermolecular interactions in the analysis of the current response of confined molecules [42]. In this reference, the authors focused their results mainly on the simplified situation of "uniform interactions" (i. e., the interaction coefficients for the different species are assumed equal), which is not a very usual experimental situation. Moreover, the authors indicated that the general situation is very complex to analyse and it is not possible to define a single parameter for accounting the effects of individual interaction coefficients. Indeed, the results of this latter study are analogous to that of a simple charge transfer process with an apparent rate constant the value of which depends on the experimental conditions (mainly on the surface coverage).

In this manuscript, we analyze the SWV response of a surface confined electroactive probe that exhibits finite kinetics by including the influence of intermolecular interactions under

conditions where the electrostatic environment of the confined molecules determines the nature of intermolecular interactions. No restrictions in the values of the interaction coefficients have been assumed. Methods for determining the kinetics and interaction parameters are proposed and applied to the electrochemical characterization of binary ferrocenylundecanethiol / decanethiol at gold electrodes at an ethanolic medium.

2. Experimental conditions

Reagents and Chemicals

Ethanol (Merck), 11-(Ferrocenyl)undecanethiol ($C_{11}H_{22}FeS$), 10-decanethiol ($C_{10}SH$), Lithium perchlorate ($LiClO_4$) (Sigma-Aldrich) and Ethanol (EtOH) (Merck) were reagent grade and used as received.

Preparation of the binary ferrocene monolayers at gold electrodes

Monolayers of ferrocene were formed by the self-assembling technique on a gold substrate. The gold electrode was mechanically polished on alumina slurry of different grain size (1, 0.3 and 0.05 μm, Buelher), washed and electrochemically cleaned by cycling the potential between 0 V and -1.4 V (vs. SCE) in 2.0 M NaOH and then between 1.6 V and 0.4 V (vs. SCE) in 1.0 M H_2SO_4 until stable voltammograms was obtained. They were then washed with ethanol and water and soaked in solutions 2 mM of 11-(Ferrocenyl)undecanethiol (FcC11SH) + 1-decanethiol (C10SH) in a proportion 1:5 (ratio V:V), for 48 h at room temperature. Upon removal from this solution, the electrode was thoroughly rinsed with ethanol and left in the organic solvent for 48 hours before use.

The resulting monolayers are very stable and no significant loss of signal is appreciated after four-five weeks.

Electrochemical measurements and data analysis

A three-electrode cell was employed in the experiments with gold disc electrodes of diameter 0.2 cm as working electrodes (CH Instruments). The counter electrode was a Pt foil, and the reference electrode was a Ag quasi-reference electrode. Solutions were prepared with absolute ethanol of reagent quality. Nitrogen gas was passed through solutions for de-aeration for 20 min prior to measurements, with nitrogen atmosphere maintained over the solution during all the experiments.

Square Wave Voltammetry (SWV) was performed using a home-made computer-driven potentiostat-galvanostat. The net SWV response corresponds to the difference of current signals obtained between two successive half-cycles measured at the end of each potential step (see Figure SI1 of the Supporting Information, SI, and [20, 27]).

The baseline correction of the experimental SWV curves was performed by fitting of the current values obtained outside the Faradaic region to a polynomial of third degree followed by subtraction by means of the “Transforms” routines of SigmaPlot 10.0 for Windows.

All experimental measures have been carried out at T=298 K with a potential step in the Square Wave potential wave form of $\Delta E_{st} = 5$ mV.

The influence of ohmic drop on the SWV response has not been considered. On the basis of previously determined values of the time cell constant and capacitance of binary ferrocene monolayers, it can be concluded that the ohmic resistance lays in the range 10-100 Ω [17, 43]. Therefore, any distortion of the voltammetric curves arising from ohmic drop could be considered as negligible.

3. Theory

Let us consider the following charge transfer process involving the surface confined electroactive species O and R at an electrode of area *A*:

$$\mathrm{R} \underset{k_{\mathrm{red}}}{\overset{k_{\mathrm{ox}}}{\rightleftarrows}} \mathrm{O} + \mathrm{e}^- \tag{I}$$

with k_{ox} and k_{red} being the rate constants for the electro-oxidation and electro-reduction processes. We will assume that the adsorbed electroactive couple O/R is in the presence of an electroinactive co-adsorbate P.

In a previous paper, we have deduced the expression for the current-potential response for process (I) in the presence of intermolecular interactions when a single constant potential *E* or a sequence of *m* consecutive constant potentials E_1, E_2, ..., E_m of the same time length τ is applied to the electrode [17]. The current corresponding to process (I) for any potential can be written as

$$\frac{I_m}{Q_{\mathrm{E}}} = -\frac{df_{\mathrm{R,m}}}{dt} \tag{1}$$

where

$$f_{\mathrm{i,m}} = \frac{\Gamma_{\mathrm{i,m}}}{\Gamma_{\mathrm{E}}}; \qquad \mathrm{i=O,\ R} \tag{2}$$

$$\Gamma_{\mathrm{E}} = \Gamma_{\mathrm{O}} + \Gamma_{\mathrm{R}} \tag{3}$$

$$Q_{\mathrm{E}} = FA\Gamma_{\mathrm{E}} \tag{4}$$

$\Gamma_{\mathrm{i,m}}$ (mol / cm^2) is the surface concentration of species i corresponding to the m-th potential pulse applied E_m. By following the procedure described in [17], the following expression for the current is obtained

$$\begin{aligned} \Phi_m = \frac{I_m\tau}{Q_{\mathrm{E}}} &= -\frac{df_{\mathrm{R},m}}{d\left(t/\tau\right)} = -\frac{df_{\mathrm{R},m}}{dT} = \\ &= \bar{k}_{\mathrm{ap}}^{0'} g\left(\eta_{\mathrm{ap},m}\right) \mathrm{e}^{-\theta_{\mathrm{E}} S f_{\mathrm{R},m}} \left(f_{\mathrm{R},m} \mathrm{e}^{\eta_{\mathrm{ap},m}} \mathrm{e}^{\theta_{\mathrm{E}} G\left(1-f_{\mathrm{R},m}\right)} - \left(1-f_{\mathrm{R},m}\right) \mathrm{e}^{\theta_{\mathrm{E}} G f_{\mathrm{R},m}} \right) \end{aligned} \tag{5}$$

where

$$\begin{aligned} &\theta_{\mathrm{E}} = \frac{\Gamma_{\mathrm{E}}}{\Gamma_{\mathrm{M}}} \\ &\Gamma_{\mathrm{M}} = \Gamma_{\mathrm{E}} + \Gamma_{\mathrm{P}} \end{aligned} \tag{6}$$

$$\left.\begin{aligned} G &= \lambda - \gamma + \beta - \mu = a_{\mathrm{OO}} + a_{\mathrm{RR}} - 2a_{\mathrm{OR}} \\ S &= \lambda - \gamma - \beta + \mu = a_{\mathrm{RR}} - a_{\mathrm{OO}} \end{aligned}\right\} \tag{7}$$

$$\eta_{\mathrm{ap}} = \frac{F}{RT}\left(E - E_{\mathrm{ap}}^{0'}\right) = \eta - \theta_{\mathrm{E}}\left(S + f_{\mathrm{P}} S_{\mathrm{P}}\right) \tag{8}$$

$$\left.\begin{aligned} E_{\mathrm{ap}}^{0'} &= E^{0'} + \frac{RT}{F}\theta_{\mathrm{E}} S + \frac{RT}{F}\theta_{\mathrm{E}} f_{\mathrm{P}} S_{\mathrm{P}} \\ S_{\mathrm{P}} &= 2\left(a_{\mathrm{RP}} - a_{\mathrm{OP}}\right) \end{aligned}\right\} \tag{9}$$

$$\bar{k}_{\mathrm{ap}}^{0'} = \bar{k}^{0'} e^{\theta_{\mathrm{E}}\left(S - G - 2a_{\mathrm{OR}}\right)} e^{-2\theta_{\mathrm{E}} a_{\mathrm{OP}} f_{\mathrm{P}}} = \bar{k}^{0'} e^{-2\theta_{\mathrm{E}}\left(a_{\mathrm{OO}} + a_{\mathrm{OP}} f_{\mathrm{P}}\right)} \tag{10}$$

$$\bar{k}^{0'} = k^{0'} \tau \tag{11}$$

a_{OO}, a_{RR}, a_{OR}, a_{OP} and a_{RP} are the interaction coefficients for couples O-O, R-R, O-R / R-O, OP and RP respectively (with a_{ij} being positive for attractions and negative for repulsions). Moreover, $g(\eta)$ is a function that defines the potential dependence of the electro-oxidation and electro-reduction rate constants, k_{ox} and k_{red}, respectively. Its particular form depends on the kinetic model chosen (i. e., Butler-Volmer, BV, or Marcus-Hush, MH). The expression of $g(\eta)$ for both models is given in Appendix I.

A simplified situation arises when we assume that the interaction coefficients of the different pairs are approximately equal [42] (uniform interactions, $a_{\mathrm{OO}} = a_{\mathrm{RR}} = a_{\mathrm{OR}} = a_{\mathrm{OP}} = a_{\mathrm{RP}} = a$), then $G = S = S_{\mathrm{P}} = 0$ such that the current-potential relationship is formally identical to that corresponding to the ideal case [17], but there is a remaining influence of intermolecular interactions on the kinetics through coefficient *a* since (see equation (10)),

$$\bar{k}_{\mathrm{ap,uniform}}^{0'} = \bar{k}^{0'} e^{-2\theta_{\mathrm{E}} a\left(1 + f_{\mathrm{P}}\right)} \tag{12}$$

which coincides with the results in reference [36] by assuming that there is no presence of electroinactive coadsorbate (i. e., $f_{\mathrm{P}} = 0$ and $\bar{k}_{\mathrm{ap,uniform}}^{0'} = \bar{k}^{0'} e^{-2\theta_{\mathrm{E}} a}$). In practice, this analysis is analogous to that of a single surface charge transfer with an apparent rate constant that depends on the parameter "*a*" (the value of which is a function of experimental factors, mainly of the surface coverage).

By applying a numerical method (for example the 4th order Runge-Kutta one, see [17]), equation (5) can be solved for a given potential waveform. Here we will apply the expression for the current given by equation (5) to calculate the response to the potential perturbation corresponding to the multipotential pulse technique Square Wave Voltammetry (SWV) given by (see also Figure S1 of the SI):

$$E_m = E_{\mathrm{initial}} - \left[\mathrm{Int}\left(\frac{m+1}{2}\right) - 1\right]\Delta E_{\mathrm{st}} - (-1)^m E_{\mathrm{SW}};\ m = 1, 2, ..., \mathrm{N} \tag{13}$$

where N is the total number of potential pulses applied, ΔE_{st} is the potential step of the staircase and E_{SW} is the square wave amplitude. Accordingly, three input parameters are necessary to be

specified in SWV measurements: ΔE_{st}, E_{SW} and the frequency (f) or the time pulse length τ, with $\tau = 1/(2f)$ (see Figure S1 of the SI).

The current (SWV) response is sampled at the end of each potential pulse and the net response (I_{SW}) is given by the subtraction of the current corresponding to a pulse with odd index (forward current) and the signal of the following pulse with even index (reverse current) [20, 27]:

$$I_{SW,c} = I_{2c-1} - I_{2c};\ c = 1, 2, ..., (N/2) \quad (14)$$

where c refers to the c-th pair of pulses or cycle and subscripts f and r to the forward ($2c-1$) and reverse (2c) components of each cycle. The SW current is plotted versus the arithmetic average of the potentials applied:

$$E_{index,c} = E_{initial} - (c-1)\Delta E_{st} \quad (15)$$

4. Results and discussion

In the following, unless indicated, the Butler-Volmer kinetics formalism will be considered.

4.1. Theoretical results

Figure 1 shows the SWV responses calculated from equations (5) and (13) for different values of the dimensionless rate constant $\bar{k}_{ap}^{0'}$, a fixed square wave amplitude of 40 mV, $\Delta E_{st} = 5$ mV, $\theta_E G = \theta_E S = 1$ and a charge transfer coefficient $\alpha = 0.5$. From the curves in this Figure we can see the typical evolution of the SWV current signal when changing the dimensionless rate constant. Thus, at the Nernstian limit corresponding to high values of $\bar{k}_{ap}^{0'}$ (see curves with $\log\left(\bar{k}_{ap}^{0'}\right) = 0.4$ and 0.25), the current shows almost negligible values and two different peaks that increase when reaching the quasi-reversible zone (see curves with $\log\left(\bar{k}_{ap}^{0'}\right) = 0.1$ and -0.25). In this region, both current peaks grow and get closer to each other till they merge into a single current peak where the highest value of the current is reached ($\log\left(\bar{k}_{ap}^{0'}\right) = -1$). When the kinetics becomes slower according to the decrease of $\log\left(\bar{k}_{ap}^{0'}\right)$, the current signal strongly diminishes keeping a single peak feature till reaching the fully irreversible region ($\log\left(\bar{k}_{ap}^{0'}\right) = -3$).

This figure shows the most typical features of SWV responses of surface confined species, i. e., the splitting of the response for intermediate values of $\log\left(\bar{k}_{ap}^{0'}\right)$ and the appearance of a maximum peak current or quasi-reversible maximum (QRM), which is a function of the dimensionless rate constant [27, 29, 42]. Note that the two peaks observed for $\log\left(\bar{k}_{ap}^{0'}\right) > -1$ are not symmetrical, with the peak located at more positive potentials being in all the cases higher than that located at more negative ones. This fact cannot be attributed to the redox kinetics since, for $\alpha = 0.5$, symmetrical quasi-reversible peaks are observed [27], and the asymmetry observed is directly related to the influence of intermolecular interactions (see below).

The maximum sensitivity for the current is obtained under quasi-reversible conditions for which the influence of the redox kinetics and intermolecular interactions on the response is also maximum. This is one of the main problems for the kinetic analysis of surface redox processes with SWV since, under these conditions, there exist a complex interplay between both sets of kinetic and interaction parameters (see below).

< Figure 1 >

In order to clearly analyse the effect of the interaction parameters $\theta_E G$ and $\theta_E S$ on the quasi-reversible SWV curves, in Figure 2 we have plotted a set of nine $\Phi_{SW} - E_{index}$ plots,

calculated for different values of E_{SW}, $\theta_E G$ and $\theta_E S$, a fixed value of the dimensionless rate constant $\left(\bar{k}_{ap}^{0'}=1\right)$, $\Delta E_{st}=5$ mV and $\alpha=0.5$.

As stated above, one of the most relevant features of the square wave voltammograms is the appearance of two peaks when the process behaves as quasi-reversible. The origin of this feature, as has been discussed in detail in [27], lays in the way the Φ_{SW} signal is recorded, since it is plotted versus an average applied potential for forward and reverse pulses, E_{index}. Whenever two peaks appear in the response, we will denote $\Phi_{SW}^{peak,-}$ and $\Phi_{SW}^{peak,+}$ to those current peaks obtained at less and more positive potentials than the apparent formal potential, respectively. $E_{SW}^{peak,-}$ and $E_{SW}^{peak,+}$ will be the potentials of each peak, $\Delta E_{SW}^{peak}=E_{SW}^{peak,+}-E_{SW}^{peak,-}$ the difference between each peak potential, and $RQ=\Phi_{SW}^{peak,-}/\Phi_{SW}^{peak,+}$ the ratio between the peak heights. The values of all these parameters for the curves in Figure 2 are given in Tables SI1-SI4 of the Supporting Information, SI.

In the curves in Figure 2 it can be seen that, under ideal conditions ($\theta_E G=\theta_E S=0$, Figure 2E), a symmetrical peak splitting appears (with $\Phi_{SW}^{peak,-}=\Phi_{SW}^{peak,+}$ and $E_{SW}^{peak,+}=-E_{SW}^{peak,-}$), so the entire signal is "centred" around the apparent formal potential [20, 27, 31]. In addition, we can see that the peak separation (ΔE_{SW}^{peak}) decreases with the square wave amplitude (E_{SW}) till both peaks start to overlap. For the SWV curves in this Figure and the particular value of the dimensionless rate constant $\left(\bar{k}_{ap}^{0'}=1\right)$, the partial overlapping of both peaks starts for $E_{SW}=100$ mV, and they fully merge into a single peak for $E_{SW}\le 40$ mV (see also Tables SI1-SI4 of the SI).

If we analyse how the interaction parameter $\theta_E G$ affects the current signal for a fixed value of the parameter $\theta_E S$, we can observe that the full width at the half maximum (fwhm) of the current peaks is larger for $\theta_E G<0$, both in split and fully overlapped signals (compare, for example, Figures 2A and 2C corresponding to $\theta_E G=-1$ and 1, respectively) . It can also be seen that, in the split signals, the peak separation (ΔE_{SW}^{peak}) decreases as $\theta_E G$ becomes negative, a fact that can be observed for example in Figure 2D and Table SI2 ($\theta_E G=-1$ and $\theta_E S=0$). In this last Figure it can be observed that, even for the largest square wave amplitude ($E_{SW}=120$ mV), the peaks are partially overlapped, and that both peaks fully merge in one peak for $E_{SW}\le 80$ mV. For $\theta_E G>0$, the opposite behaviour is obtained, with the peaks being narrower and with a higher separation (ΔE_{SW}^{peak}) (i. e., the split signal appears for lower values of E_{SW}, see Figure 2F and Table SI2).

Regarding the effect of the interaction parameter $\theta_E S$ on the SWV signal for a fixed value of the parameter $\theta_E G$, it is clear that when $\theta_E S \neq 0$ the current is not centred around $E_{index} = E_{ap}^{0'}$, with the SWV curves being displaced from $E_{index} = E_{ap}^{0'}$ towards more positive values when $\theta_E S < 0$, whereas the opposite behaviour is observed for $\theta_E S > 0$ (see for example Figures 2G and 2I and Table SI2). Moreover, condition $\Phi_{SW}^{peak,-} < \Phi_{SW}^{peak,+}$ (i. e., $RQ < 1$) is fulfilled for negative values of $\theta_E S$ whereas RQ is higher than unity for $\theta_E S > 0$. Thus, from a simple glance of the $\Phi_{SW} - E_{index}$ curves, it is possible to estimate qualitatively the sign and magnitude of $\theta_E S$.

Concerning the values of the peak heights, they decrease for $\theta_E S < 0$ (for example, Φ_{SW}^{peak} values for $\theta_E S = -1$ are around one half of those obtained $\theta_E S = 0$), whereas the contrary effect is observed for $\theta_E S > 0$ (with Φ_{SW}^{peak} values for $\theta_E S = 1$ being around twice those obtained for $\theta_E S = 0$). Also, as mentioned before, the appearance of split current signals for smaller values of E_{SW}, takes place at higher values of the square wave amplitude for $\theta_E S < 0$ (being around 15mV larger for $\theta_E S = -1$ when compared with $\theta_E S = 0$), and the contrary is observed for $\theta_E S > 0$ (being around 30 mV smaller for $\theta_E S = 1$ when compared with $\theta_E S = 0$).

< Figure 2>

Figure 2 clearly shows that the SWV current is strongly affected by both $\theta_E G$ and $\theta_E S$ parameters, especially at the asymmetrical splitting region. This complex landscape cannot be obtained if uniform interactions are assumed in the way done in [42]. As will be seen below, this region is recommended for carrying out the determination of the rate constant of the charge transfer process under study. Thus, it will be very useful to have a broad range of $\bar{k}_{ap}^{0'}$ for which a split SWV signal could be obtained. This can be achieved by using high values of the square wave amplitude E_{SW} as shown in Figure SI2 of the SI, obtained for $\theta_E G = 1$ and $\theta_E S = -1$. The SWV curves in this Figure show that for $E_{SW} = 120$ mV it is possible to obtain a split SWV response for $\log\left(\bar{k}_{ap}^{0'}\right) \geq -1.145$, showing both SWV peaks a ratio $0.6065 \geq RQ \geq 0.4752$. When smaller pulse amplitude values are used, for example for $E_{SW} = 40$ mV, the split region is narrower and values of $\log\left(\bar{k}_{ap}^{0'}\right) \geq -0.320$ are required. Note that the asymmetry degree in the SWV response depends on parameter $\theta_E S$ (and therefore on those experimental conditions that lead to changes in this parameter as, for example, the surface amount of redox probe or the electrolytic media), and it cannot be justified unless non-uniform interactions are considered (see for example [42, 44]).

Due to the fact that the main application of these curves is the determination of the rate constant using the location of the QRM [27, 28, 42, 44], it is important to analyse the impact of the interaction parameters on it. In Figures 3 and SI3 of SI we have plotted the $\Phi_{SW}^{peak} - \log\left(\overline{k}_{ap}^{0'}\right)$ curves obtained for $\Delta E_{st} = 5$ mV, a fixed $\theta_E G$ and three values of $\theta_E S$ (Figure 3), and for a fixed $\theta_E S$ and three values of $\theta_E G$ (Figure SI3). In all cases, the value of the square wave amplitude is $E_{SW} = 40$ mV.

In both Figures we can observe how a positive value of $\theta_E G$ give rises to the increase of the value of the QRM current (being for $\theta_E G = 1$ around 57% higher than that corresponding to $\theta_E G = 0$), while negative values of $\theta_E G$ cause a decrease of the QRM (being for $\theta_E G = -1$ around 29% smaller when compared with that obtained for $\theta_E G = 0$). The appearance of asymmetric split signals is more evident for positive values of $\theta_E G$ and it corresponds to values of the apparent rate constant in the region $\left(-0.4 \le \log\left(\overline{k}_{ap}^{0'}\right) \le 0.8\right)$ (see Figure 3c).

Concerning the values of the rate constant that can be obtained from the measurement of the QRM, it can be seen that, for positive values of $\theta_E G$ and a fixed value of $\theta_E S$ (Figure 3C), the QRM appears at more positive values of $\log\left(\overline{k}_{ap}^{0'}\right)$. This fact could lead to the underestimation of the rate constant if the effect of interactions is not considered (around 20% smaller compared with that corresponding to $\theta_E G = 0$), whereas the opposite effect is observed for negative values of $\theta_E G$ (with values of $\log\left(\overline{k}_{ap}^{0'}\right)$ obtained from QRM measurements around 20% bigger compared with those obtained for $\theta_E G = 0$). Based on these deviations, it is clear that $\theta_E G$ is a key parameter that should be known in order to make reliable kinetic measurements with SWV.

Regarding the effect of $\theta_E S$ on the location of QRM and, therefore, in the estimation of the rate constant (Figure SI2), it can be observed that, for positive values of $\theta_E S$ the QRM appears at more positive values of $\log\left(\overline{k}_{ap}^{0'}\right)$. This result leads to the overestimation of the rate constant (around 70% bigger compared with that obtained for $\theta_E S = 0$), whereas for negative values of $\theta_E S$ the contrary effect is observed, ($\log\left(\overline{k}_{ap}^{0'}\right)$ values around 35% smaller compared with those corresponding to $\theta_E S = 0$).

In the worst scenario, where the electroactive monolayer presents values of $\theta_E G < 0$ and $\theta_E S > 0$, the wrong estimation of the rate constant by analysing the signal without taking into account the effects of the interactions, can lead to artificially double its value.

< Figure 3 >

Indeed, the values of $\theta_E G$ and $\theta_E S$ are very important when defining intervals of reversibility for the surface redox probe, i.e., ranges of values of the apparent dimensionless rate constants from which it could be possible to identify the response of the charge transfer process as reversible, quasi-reversible or fully irreversible. Thus, in the same way that the QRM changes with the interaction parameters $\theta_E G$ and $\theta_E S$ (see Figures 3 and SI2), the limits of the different reversibility regions (reversible, quasi-reversible or irreversible) change as well. In order to be able of identifying them correctly, we have plotted in Figure 4 two examples showing the different regions of the signal for different values of the interaction parameters ($\theta_E G$ and $\theta_E S$) and a fixed value of $E_{SW} = 40$ mV.

In this Figure we have considered that the signal falls in the reversible zone when the current peak height is below 5% of the QRM, and that can be considered in the irreversible region when the current is lower than 105% of the fully irreversible maximum current. As we can see in this figure the limits of these regions move when changing $\theta_E G$ and $\theta_E S$. Therefore, we should always know the values of the interactions parameters in order to be able to properly classify the experimental response into a given reversibility region. Of special interest is the $\bar{k}_{ap}^{0'}$ interval for which two symmetric or asymmetric current peaks are obtained (see for example the $\left(-0.4 \le \log\left(\bar{k}_{ap}^{0'}\right) \le 0.8\right)$ region in Figures 3C and 4B corresponding to $\theta_E G = 1$ and $\theta_E S \neq 0$), since under these conditions the determination of kinetic and interaction constants is easier (see below).

< Figure 4 >

As stated in previous sections, the theoretical framework used for the analysis of the SWV response does not require an a priori kinetic formalism as in the CV case. Thus, up to now, we have employed the more usual BV one but its replacement by the MH one is immediate by simply changing the function $g\left(\eta_{ap,m}\right)$ in equation (5) (see also equations (A1)-(A3) in Appendix). In order to analyse the differences between both the BV and MH formalisms, we have plotted in Figure 5 a set of SWV curves calculated for different values of $\theta_E G$ and $\theta_E S$ (values shown in the Figure), and $\bar{k}_{ap}^{0'} = 1$ for both the BV (solid lines) and symmetrical MH (dashed lines) formalisms, calculated for a square wave amplitude $E_{SW} = 40$ mV. We have considered a value of $\alpha = 0.5$ for the BV curves and a dimensionless molar reorganization energy $\Lambda = 30$ for the MH ones (this is a typical value for functionalized alkanethiols on gold, see [17, 45]), and a symmetry factor $\gamma = 0$ [46]. The corresponding forward and reverse currents for the case $\theta_E G = -1$ are also given in Figure SI4 of the SI. As can be seen in these curves, the differences

between both types of kinetic formalisms is very small, with errors in the peak currents below 4% in all the cases. The major differences correspond to negative values of $\theta_E G$ and positive values of $\theta_E S$ (see black lines in Figure 5c). Thus, under these conditions (values of $\Lambda \geq 30$), the kinetic analysis of surface confined charge transfer processes with SWV could be carried out by using the BV model. The differences between both BV and MH kinetic formalisms will be more evident for systems with small rate constants and reorganization energies, for which high overpotentials are required to observe their redox behaviour [45, 46]. On the other hand, for values of $\bar{k}_{ap}^{0'} \geq 0.1$ the differences between both formalisms are small, as can be seen in Figure SI5 of the SI, corresponding to a charge transfer process with $\bar{k}_{ap}^{0'} = 0.1$, $\theta_E G = 1$, $\theta_E S = -1$, $E_{SW} = 40$ mV and $\Delta E_{st} = 5$ mV. Thus, the decrease of Λ in the range $40 \leq \Lambda \leq 20$ (i. e., $1 \leq \lambda \leq 0.5$ eV), gives rise to slightly broader SWV responses, with a maximum difference in the currents obtained for BV and MH formalisms below 5%.

< Figure 5 >

As a summary, in order to carry out kinetic measurements of a given surface redox probe with SWV, we should bear in mind the complex behaviour arising when quasi-reversible conditions are considered since the mutual influences of kinetic and interaction parameters is maximum. Thus, on the basis of the above results it can be concluded that the optimal way to fully characterise the redox kinetics of a given surface confined redox species requires the a priori knowledge of parameter $\theta_E G$. This can be done from the measurement of the charge-potential curves by using SWVC in the way discussed in reference [40]. From the charge-potential curves it is also possible to obtain in a very easy way the value of the apparent formal potential and the surface coverage. Once $\theta_E G$ is known, the following operating procedure is proposed (see also the diagram in Figure 6): firstly, the apparent rate constant $k_{ap}^{0'}$ can be estimated by overlapping the experimental peak heights of the SWV curves to a theoretical $\Phi_{SW}^{peak} - \log(\tau)$ curve, assuming a value of $\theta_E S \approx 0$ (and being aware of the error of this estimation, which is, as stated above, between 85%-170% of the real value). Next, we can determine $\theta_E S$ using the peak separation $\left(\Delta E_{SW}^{peak}\right)$ of the SWV response under experimental conditions for which a clear splitting of the current is obtained (see Figure 2 and Table SI2). The peak separation is an experimental parameter very sensitive to $\theta_E S$ and the square wave amplitude value, as shown in Figure SI6, obtained for $\bar{k}_{ap}^{0'} = 1$, $\theta_E G = 1$ and three E_{SW} values. Then, this new value of $\theta_E S$ is employed to correct the previously estimated apparent rate constant. Finally, we should consider possible changes in the value of α in order to carry out the final fitting of the SWV curves, if the ratio between the peak currents (RQ) does not match the response. Note that, up to now, we have assumed a typical

value of $\alpha = 0.5$ in all the cases. The influence of the charge transfer coefficient on the SWV curves under quasi-reversible kinetic conditions is small for $0.3 \leq \alpha \leq 0.7$ (see Figure SI7, obtained for different values of $\theta_E G$ and $\theta_E S$, and [27, 29]), and a fully irreversible behaviour is required to detect a strong influence of the charge transfer coefficient. Note also in Figure SI6 that the split region obtained for the ideal case ($\theta_E G = \theta_E S = 0$) is much narrower than that obtained when interactions are present.

In the case of the MH formalism, the above described process is the same but the final step corresponds to changing the reorganization energy Λ, if necessary. A final check by carrying out the overlapping of theoretical and experimental curves should certify the reliability of the fitting parameters.

< Figure 6 >

3.2 Experimental results

We have applied the methodology described above to the analysis of the square-wave current-potential responses of a binary monolayer of ferrocenylundecanethiol/decanethiol (FcC11SH/C10SH) at polycrystalline gold electrode in EtOH / $LiClO_4$ 0.1M media. This monolayer has been prepared by using a mixture of ethanolic solution 1mM of the redox probe 11-(ferrocenyl)-undecanethiol and electroinactive 1-decanethiol in the ratio (v/v) 1:5 (see experimental section for more details). We will consider in our treatment that, due to the low coverage of ferrocene probes under our experimental conditions, there is a single type of ferrocene moiety at the monolayer. Therefore, any non-ideality affecting the redox performance of the ferrocene probes in the SWV curves will be assigned to the presence of intermolecular interactions [17].

Figure 7 shows the experimental dimensionless current-potential curves $(\Phi - E_{index})$, with $\Phi = (I_{SW}\tau)/Q_E$, corresponding to the direct anodic scan obtained for E_{SW}=40 mV, $\Delta E_{st} = 5$ mV and three different pulse lengths, 20, 30 and 40 ms (i. e., frequencies in the range 10-25 Hz). We have used the value of $Q_E = 0.365$ μC determined by Square Wave Voltcoulommetry in the way discussed in [43] (see below). As can be seen in this Figure, the SWV curves correspond to the quasi-reversible region, with the current increasing as the time pulse decreases (or the frequency increases), due to the decrease of the dimensionless rate constant, $\bar{k}_{ap}^{0'} = k_{ap}^{0'}\tau = k_{ap}^{0'}/(2f)$, in line with theoretical curves in Figure 1. The SWV curves show in all the cases two asymmetric peaks, being $I_{SW}^{peak,-} < I_{SW}^{peak,+}$ with a practically constant value of $RQ \cong 0.74$, a fact that suggest that $\theta_E G > 0$ and $\theta_E S < 0$ (see Figure 2).

< Figure 7 >

Figure 8 shows a set of experimental SWV curves obtained for the three pulse lengths above mentioned (20, 30 and 40 ms) and different values of the square wave amplitude ranging from 40 to 100 mV (solid lines). As can be seen in this Figure, the split peak shape $\Phi_{SW} - E_{index}$ responses show a peak separation $\left(\Delta E_{SW}^{peak}\right)$ that increases with the square wave amplitude E_{SW}. Also, they show an almost constant value of height of both peaks, and therefore a constant value of the ratio RQ between them, for the different E_{SW} values. The clear splitting of the response and the high asymmetry observed in all the cases under these conditions have led us to focus on this quasi-reversible zone for carrying out the quantitative analysis of the response.

In order to determine the kinetic and interaction parameters of this system, we have first applied SWVC to the FcC11SH/C10SH monolayers in EtOH / $LiClO_4$ 0.1M media by using long pulse times (50 and 100 ms, i. e., frecuencies of 5 and 10 Hz) obtaining the charge-potential curves shown in Figure SI8 of the SI. From the values of the fwhm and peak charges of these curves, by carrying out the fitting process described in [40], the following experimental values have been determined: $\theta_E G = 0.89$, $E_{ap}^{0'} = 0.400$ V and $Q_E = 0.365$ μC.

Once the value of $\theta_E G$ is known, we have applied the fitting protocol described in Figure 6 for the Butler-Volmer formalism, to the experimental curves. Three iterations have been required for obtaining adequate values of the apparent rate constant and parameter $\theta_E S$ (see Figure SI9 of the SI). First, by assuming a seed value of $\theta_E S = -0.2$ and $\theta_E G = 0.89$, we have obtained theoretical $\Phi_{SW}^{peak} - \log\left(\overline{k}_{ap}^{0'}\right)$ curves for different values of the square wave pulse amplitude, and we have obtained a first $k_{ap}^{0'}$ value from the best fittings of the experimental peak heights ($k_{ap,1}^{0'}$). From the ΔE_{SW}^{peak} values of the theoretical curves for $k_{ap,1}^{0'}$ we have calculated a second $\theta_E S$ estimation ($\theta_E S = -0.7$) and generated again theoretical $\Phi_{SW}^{peak} - \log\left(\overline{k}_{ap}^{0'}\right)$ curves for comparing with the experimental values. After three iterations the values of $k_{ap}^{0'}$ and $\theta_E S$ are self-consistent and correspond to $\theta_E S = -0.61$ and $k_{ap}^{0'} = 44$ s^{-1}, by assuming $\alpha = 0.5$. Figure 9 shows the comparison between theoretical and experimental peak heights for two values of the square wave amplitude (40 and 60 mV). The value of $k_{ap}^{0'}$ is in line with previously reported ones for similar binary monolayers in non-aqueous solvents (see [17] and references therein).

The theoretical SWV curves calculated by using the estimated interaction parameters (lines) fit satisfactorily all the experimental curves for the different square wave amplitudes and time pulses shown in Figure 8. It is worth to mention the discrepancy observed in the valley between both peaks, which could be related with a double layer contribution to the response, which has not been correctly removed with the baseline correction procedure.

< Figure 8 > < Figure 9 >

The QRM of the SWV current for the interaction parameters of FcC11SH/C10SH monolayers in this media corresponds to $\log\left(\overline{k}_{\mathrm{ap}}^{0'}\right) = -0.510$ (see the Φ_{peak}-$\log\left(\overline{k}_{\mathrm{ap}}^{0'}\right)$ curve in Figure 9. If the effect of interactions was not taken into account, i. e., under $\theta_{\mathrm{E}}G = \theta_{\mathrm{E}}S = 0$ conditions, the QRM corresponds to $\log\left(\overline{k}_{\mathrm{ap}}^{0'}\right) = -0.325$, which would lead to an apparent rate constant $k_{\mathrm{ap}}^{0'} = 70\ \mathrm{s}^{-1}$, i. e., a 53% higher value.

The application of this fitting protocol has enabled us to obtain both set of interactions and kinetic parameters for this system under conditions of strong influence of intermolecular interactions.

Conclusions

The two-dimensional structure resulting from the confinement of a given redox probe is usually very complex. Unless, very demanding synthetic procedures were followed, its particular redox performance is strongly conditioned by its local surrounding energy landscape. Even under these conditions, the analysis of the redox kinetics of surface confined probes with electrochemical techniques as Cyclic Voltammetry and Square Wave Voltammetry, is typically carried out by using ideal models. These models are not able to reproduce the complex influence of the molecular environment on the conversion of the redox probes, and lead to inaccurate and irreproducible values for the kinetic parameters. This could be avoided by incorporating the influence of non-idealities in the electrochemical responses of these redox probes.

The physical origin of non-idealities is diverse, although is usually related with structural factors. We have focused our analysis on the case of intermolecular interactions since they are intrinsically related with the redox conversion. The appearance of other sources of non-ideality as, for example, the presence of thermodynamic or kinetic dispersion [25], is typically related with the existence of different structural (and therefore functional) domains in the monolayer, which corresponds to the presence of adsorbated species of large size or to high coverages of the redox probes. In the case of ferrocene monolayers, dispersion appears for values of surface coverage above 30% ([17] and references therein). Thus, since low coverages have been used here, we have assumed that the only source of non-idealities in the electrochemical response is the presence of interactions.

In particular, when intermolecular interactions effects are included in the analysis of current-potential SWV responses, significant deviations in the main features of the current-potential curves, as compared with those predicted by ideal models, are found. The estimation of the rate constant of a surface charge transfer process from measurements of the location of QRM is seriously compromised by the influence of interaction parameters $\theta_E G$ and $\theta_E S$, which distort the Φ_{peak}-$\log\left(\overline{k}_{ap}^{0'}\right)$ curves and can lead to important errors in the estimation of kinetic parameters. Thus, the rate constant estimation method based on the measurement of a single parameter as the location of QRM, which is seriously affected by the presence of intermolecular interactions under quasi-reversible redox conditions, could lead to important errors in $\overline{k}_{ap}^{0'}$. When uniform interactions are considered, the reliability of this method is restored, but this is an infrequent experimental situation. Indeed, the asymmetry in the SWV split response is usually attributed to charge transfer values far from 0.5, but in many cases this assumption cannot totally justify the deviations observed. The method proposed here, although more complex, allows to analyze the response under different experimental conditions and it provides self-validated values for the redox and interaction parameters. It should be noted that, in fact, we need to use both Square Wave Voltammetry and Voltcoulommetry since any of them separately does not provide

enough information for the complete characterization of the redox process. For example, Square Wave Voltcoulommetry allows to determine easily the sign and magnitude of the parameter $\theta_E G$ but it does not give any information about the parameter $\theta_E S$ [43]. Nevertheless, it is important to remind that differential pulse techniques as those mentioned above, are able to provide detailed insight into the electrochemical behavior of these systems under non-ideal conditions.

In this sense, we believe that the procedures presented constitute a more direct and sound methodology for the analysis of the complex landscape of redox processes of surface confined probes.

Acknowledgements

The authors greatly appreciate the financial support provided by the Fundación Séneca de la Región de Murcia (Project 19887/GERM/15).

Supporting information

The contents of the supporting information are: experimental details, potential waveform for Square Wave Voltammetry and additional theoretical and experimental results

Appendix. Expressions for function $g(\eta)$ for the BV and MH kinetics formalisms.

The expressions of function $g(\eta)$ are the following

$$g(\eta)=\begin{cases} g^{\mathrm{BV}}(\eta)=\mathrm{e}^{-\alpha\eta} \\ g^{\mathrm{MH}}(\eta)=\dfrac{F(\eta,\Lambda)}{F(0,\Lambda)}=\dfrac{\int_{-\infty}^{\infty}\left(\dfrac{\mathrm{e}^{-\Delta G_{\mathrm{red}}^{\neq}(\varepsilon,\eta,\Lambda,\gamma)}}{1+\mathrm{e}^{-\varepsilon}}\right)d\varepsilon}{\int_{-\infty}^{\infty}\left(\dfrac{\mathrm{e}^{-\Delta G_{\mathrm{red}}^{\neq}(\varepsilon,0,\Lambda,\gamma)}}{1+\mathrm{e}^{-\varepsilon}}\right)d\varepsilon} \end{cases} \tag{A1}$$

In Eq., $k^{0\prime}$ is the conditional rate constant, α is the charge transfer coefficient, and

$$\Delta G_{\mathrm{red}}^{\neq}(\varepsilon,\eta,\Lambda,\gamma)=\frac{\Lambda}{4}\left(1+\frac{\eta+\varepsilon}{\Lambda}\right)+\gamma\left(\frac{\eta+\varepsilon}{4}\right)\left(1+\left(\frac{\eta+\varepsilon}{\Lambda}\right)^{2}\right)+\gamma\frac{\Lambda}{16} \tag{A2}$$

Λ is the dimensionless reorganization energy given by

$$\Lambda=\frac{\lambda}{RT} \tag{A3}$$

where λ is the molar reorganization energy [45, 46], and γ is the asymmetry parameter that accounts for differences between the inner-shell force constants of the oxidized and the reduced species (a positive γ value is associated with greater force constants for the oxidized species and the opposite for negative γ values). The case $\gamma=0$ (equal force constants for both reduced and oxidized states) corresponds to the simpler symmetrical Marcus-Hush model. Note that for both MH and BV kinetic formalisms it is fulfilled that

$$\frac{k_{\mathrm{ox}}}{k_{\mathrm{red}}}=\mathrm{e}^{\eta} \tag{A4}$$

Figures

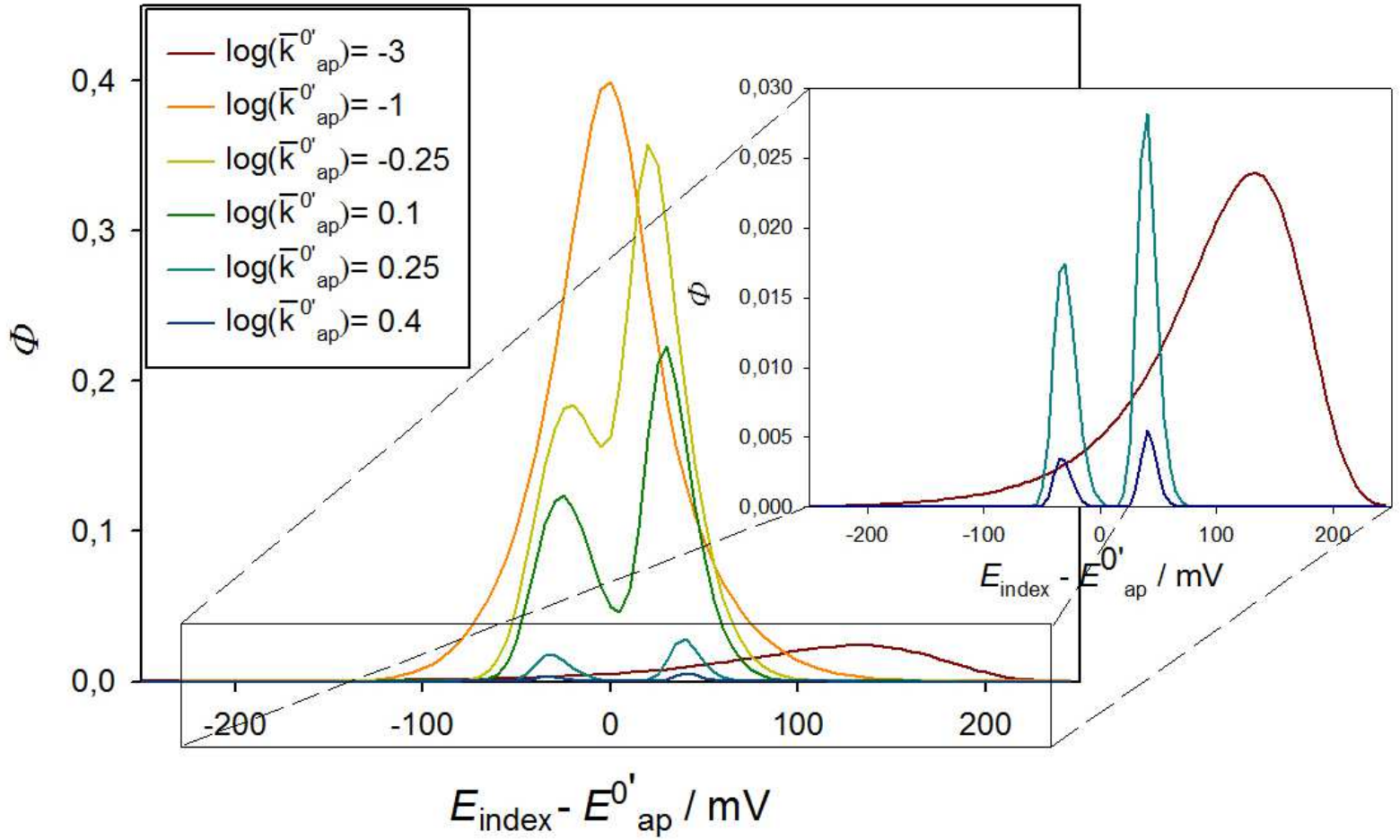

Figure 1. Theoretical SWV responses calculated from equations (5) and (13) for different values of the dimensionless rate constant $\bar{k}_{ap}^{0'}$ (shown in the curves), $E_{SW} = 40$ mV, $\Delta E_{st} = 5$ mV, $\theta_E G = \theta_E S = 1$, $\alpha = 0.5$ and T=298.15 K.

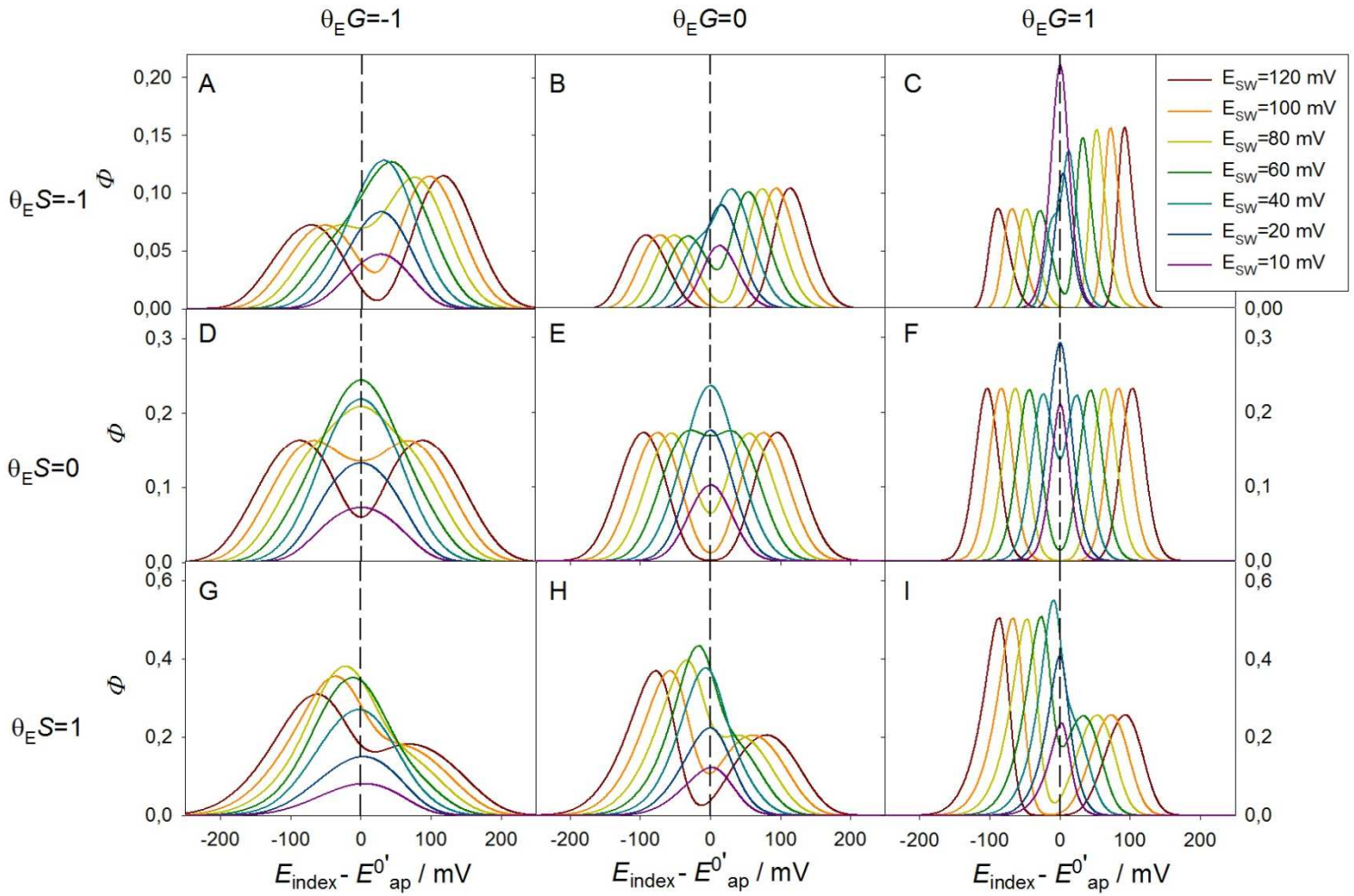

Figure 2. Theoretical SWV responses calculated from equations (5) and (13) for different values of $\theta_E G$ and $\theta_E S$ (shown in the curves). $\Delta E_{st} = 5$ mV, $\bar{k}_{ap}^{0'} = 1$, $\alpha = 0.5$ and T=298.15 K. The values of the square wave amplitude E_{SW} (in mV) are shown in the Figure.

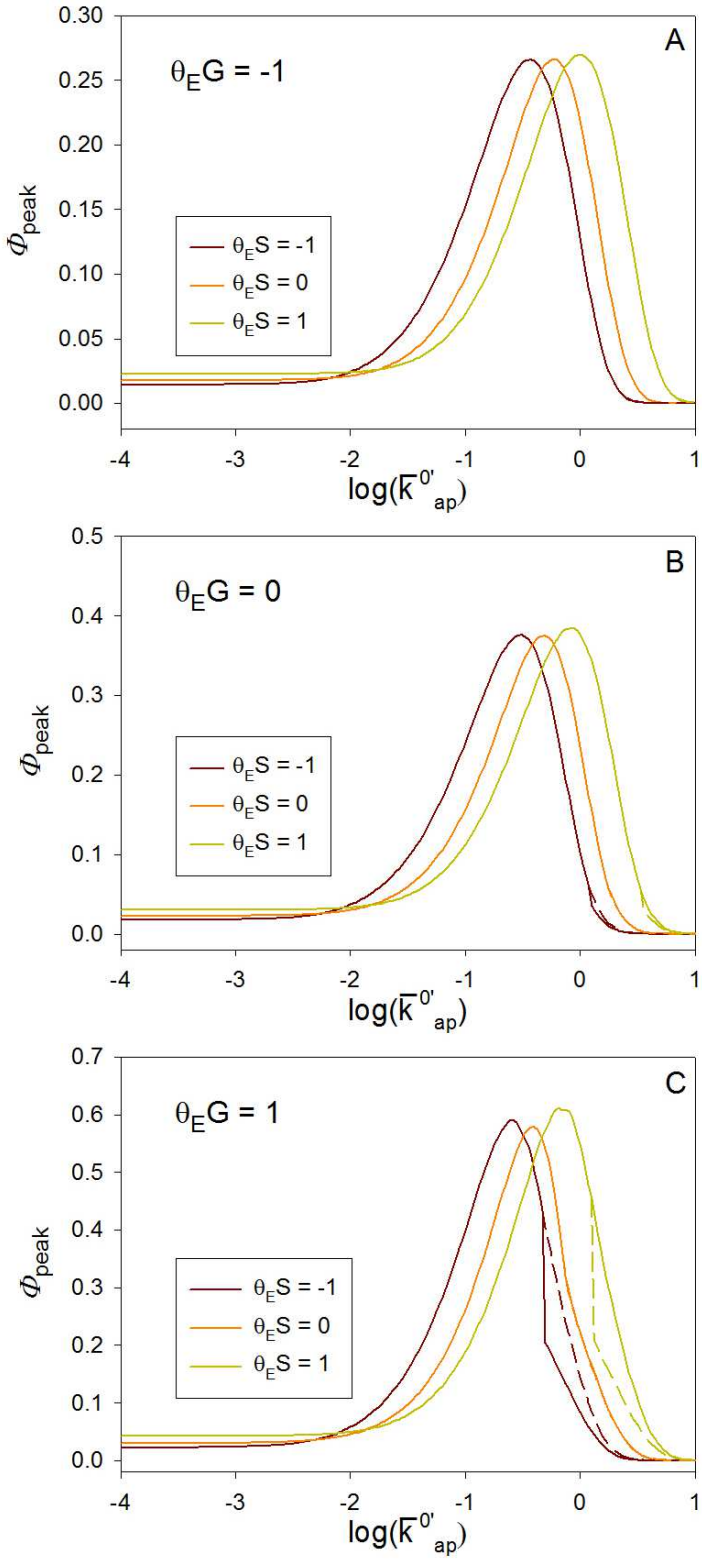

Figure 3. Theoretical $\Phi_{SW}^{peak} - \log\left(\bar{k}_{ap}^{0'}\right)$ curves calculated from equations (5) and (13) obtained for a fixed $\theta_E G$ and three values of $\theta_E S$ (shown in the curves). $E_{SW} = 40$ mV, $\Delta E_{st} = 5$ mV, $\alpha = 0.5$ and T=298.15 K. Dashed and solid lines correspond to $\Phi_{SW}^{peak,-}$ and $\Phi_{SW}^{peak,+}$, respectively, i. e., to those current peaks obtained at less and more positive potentials than the apparent formal potential, respectively.

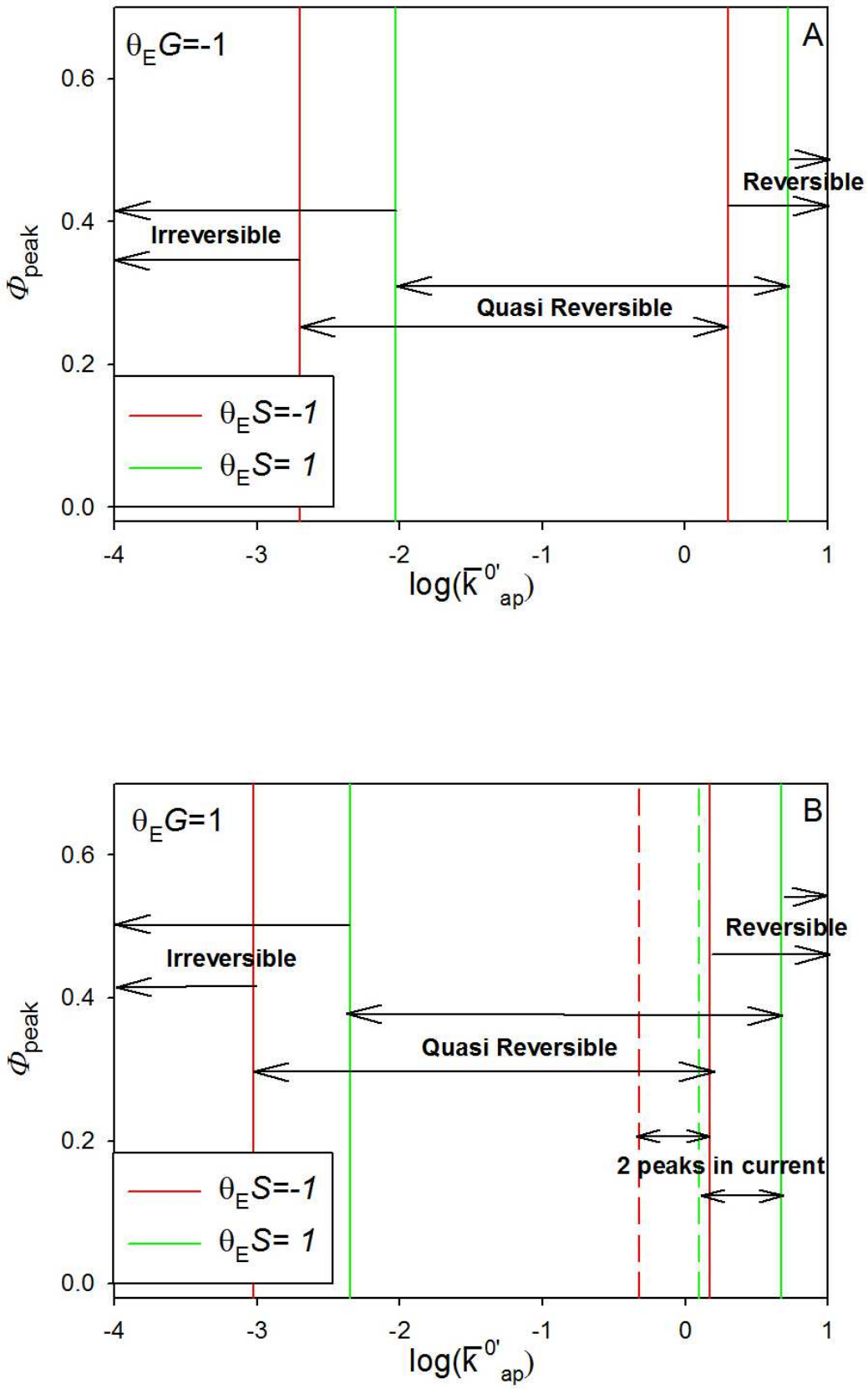

Figure 4. Reversibility regions for a simple charge transfer obtained from the measurement of the peak heights of the SWV curves calculated from equations (5) and (13) obtained for a fixed $\theta_E G$ and two values of $\theta_E S$ (shown in the curves). $E_{SW} = 40$ mV, $\Delta E_{st} = 5$ mV , $\alpha = 0.5$ and T=298.15 K

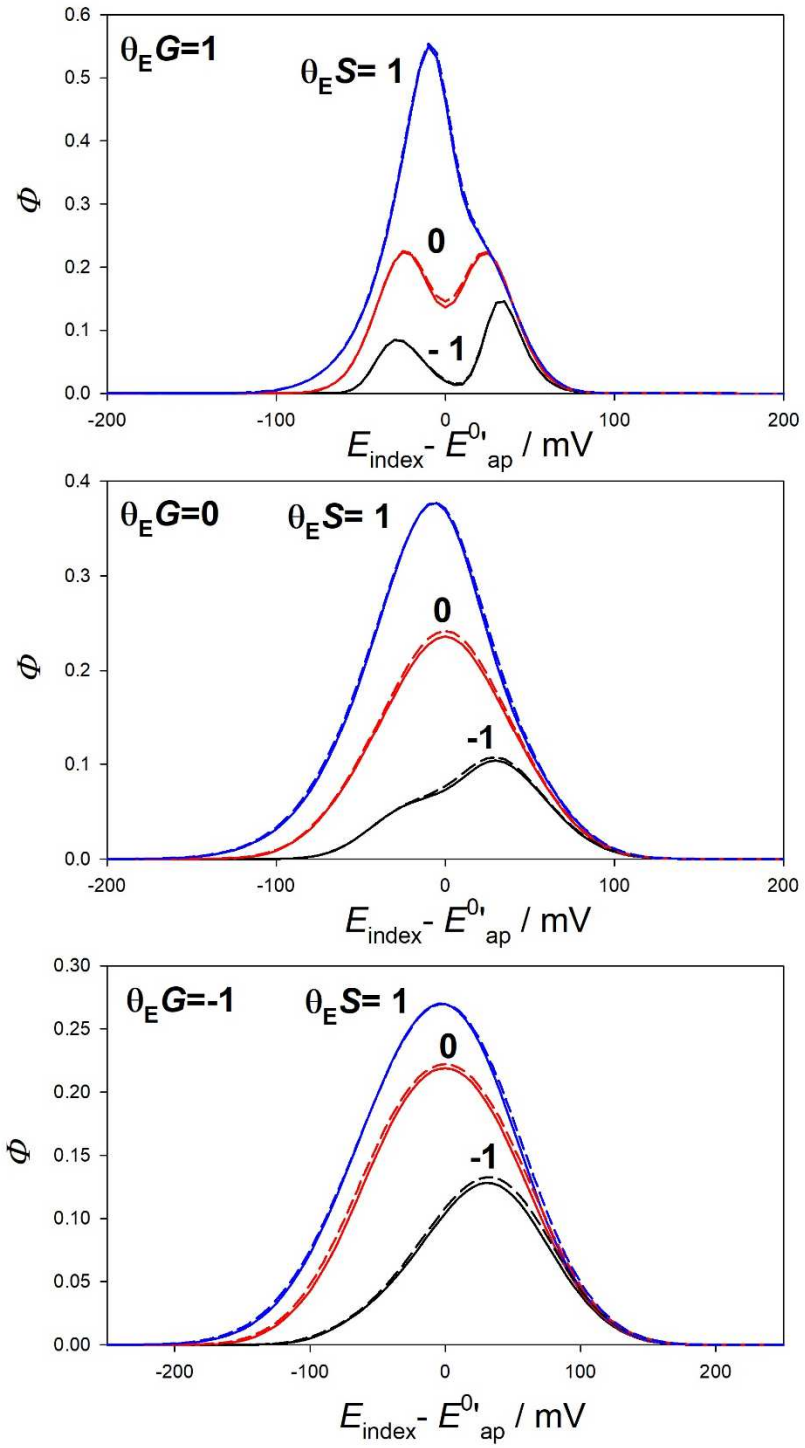

Figure 5. Theoretical SWV responses calculated from equations (5) and (13) for different values of the interaction parameters $\theta_E G$ and $\theta_E S$ (values shown in the curves) and two kinetic formalisms: Butler-Volmer (solid lines, $\alpha = 0.5$) and symmetrical Marcus-Hush (dashed lines, $\Lambda = 30$) $\overline{k}_{ap}^{0'} = 1$, $E_{SW} = 40$ mV, $\Delta E_{st} = 5$ mV and T=298.15 K

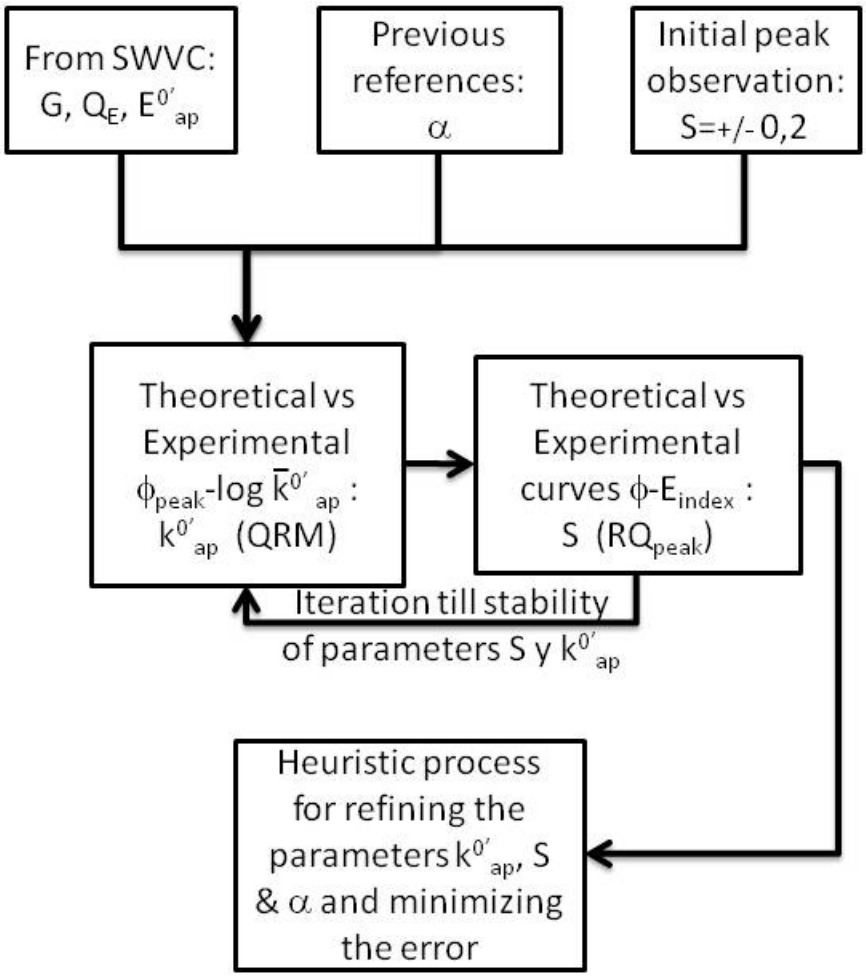

Figure 6. Scheme for the determination of kinetic and interaction parameters of a surface confined charge transfer process by using SWV.

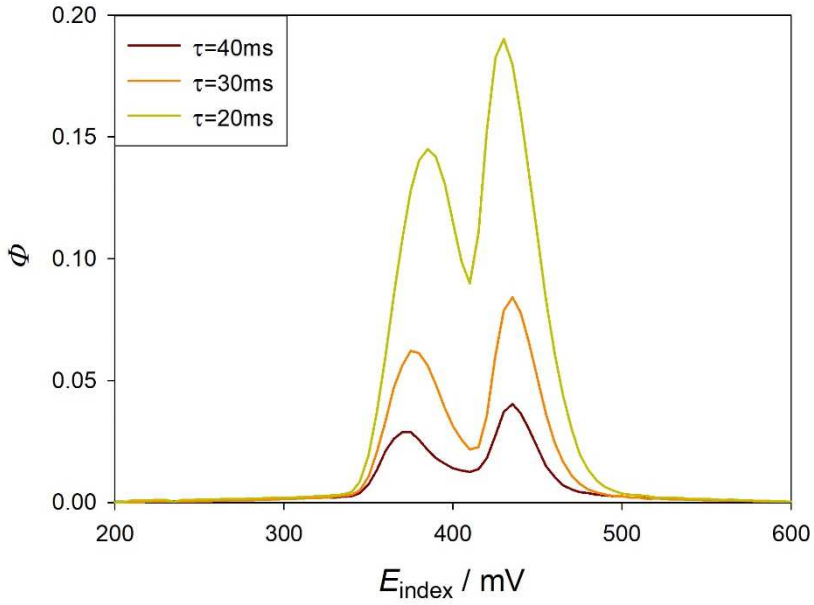

Figure 7. Experimental baseline corrected dimensionless SWV curves for the direct anodic scan corresponding to binary ferrocenylundecanethiol/decanethiol (FcC11SH/C10SH) monolayers at polycrystalline gold electrode of radius=1 mm. $\Phi = (I_{SW}\tau)/Q_E$, EtOH / ClO_4Li 0.1 M. $E_{initial} = 200$ mV, $E_{SW} = 40$ mV, $\Delta E_{st} = 5$ mV, $Q_E = 0.365$ μC. The values of the pulse length in ms are given on the curves. *T*=298 K

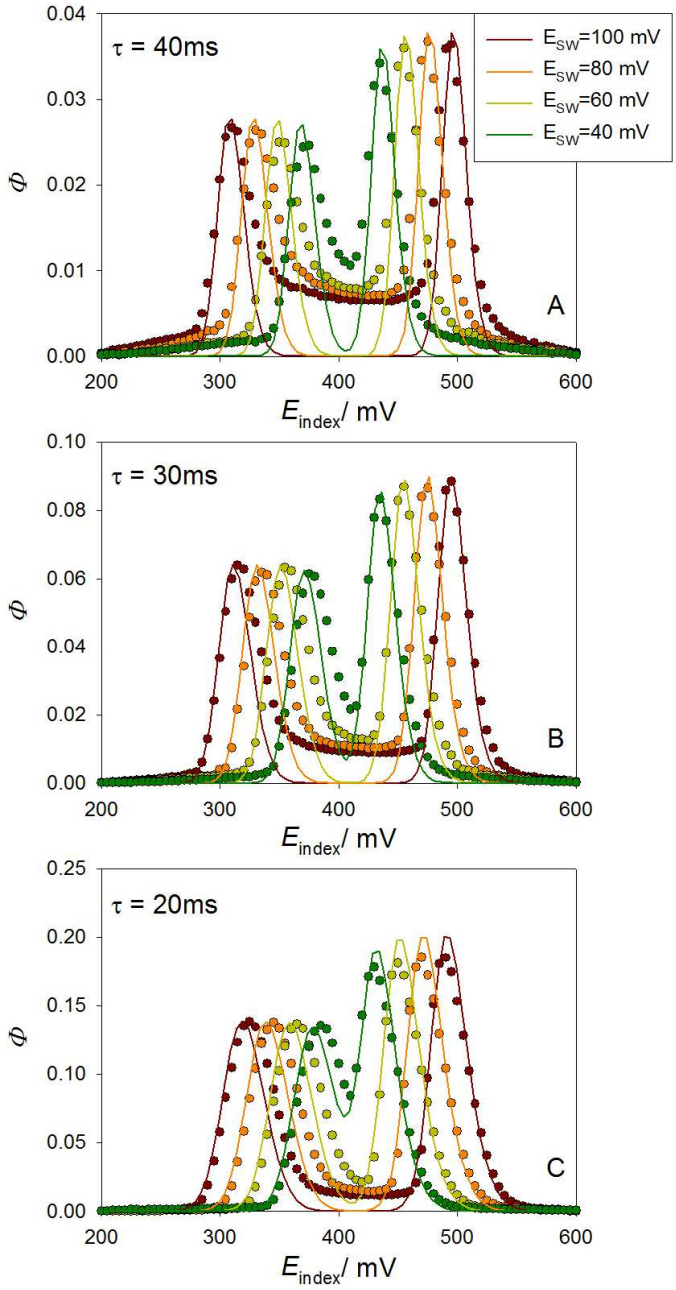

Figure 8. Symbols: experimental baseline corrected SWV curves for the direct anodic scan corresponding to binary ferrocenylundecanethiol/decanethiol (FcC11SH/C10SH) monolayers at a polycrystalline gold electrode of radius=1 mm. EtOH / ClO_4Li 0.1 M. $E_{initial} = 0$ mV, $\Delta E_s = 5$ mV T=298 K. Lines: Theoretical SWV curves for the direct anodic scan calculated from Eqns. (5) and (13) by using the following data: $\Delta E_{st} = 5$ mV, $\theta_E G = 0.89$, $E_{ap}^{0'} = 0.400$ V and $Q_E = 0.365$ μC, $\theta_E S = -0.61$ and $k_{ap}^{0'} = 44$ s^{-1}, $\alpha = 0.5$, T=298 K. The values of the pulse length (in ms) and of the square wave amplitude are (in mV) are given in the curves.

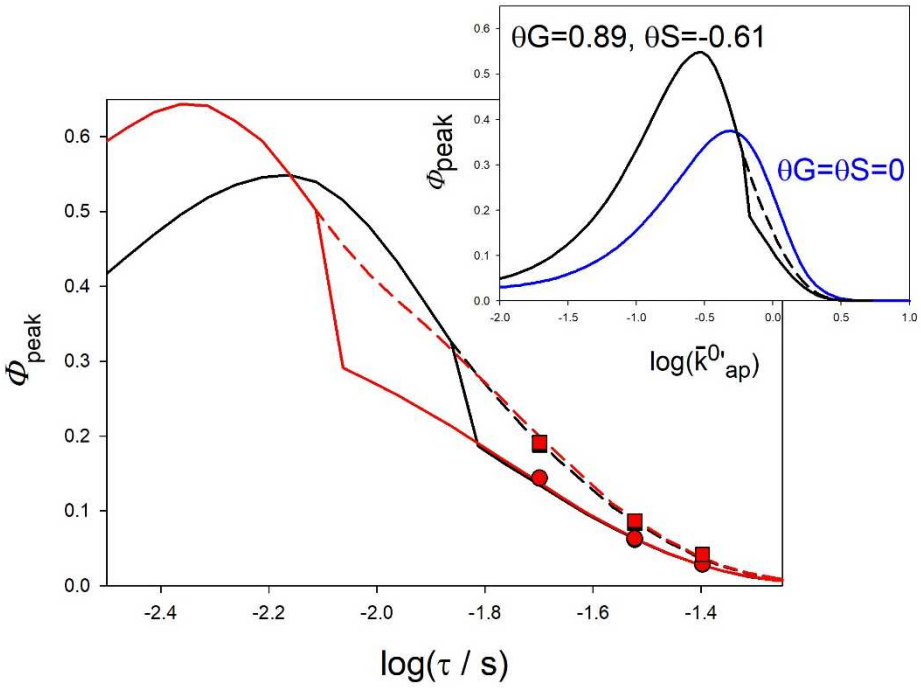

Figure 9. Symbols: experimental baseline corrected SWV peak current values for the direct anodic scan corresponding to binary ferrocenylundecanethiol/decanethiol (FcC11SH/C10SH) monolayers at a polycrystalline gold electrode of radius=1 mm. EtOH / ClO_4Li 0.1 M. Three pulse time lengths have been considered: $\tau = 20$, 30 and 40 ms. $E_{initial} = 0$ mV, $\Delta E_s = 5$ mV T=298 K. Lines: Theoretical $\Phi_{SW}^{peak} - \log(\tau)$ curves calculated from equations (5) and (13) for SWV curves for $\theta_E G = 0.89$ and $\theta_E S = -0.61$, $\Delta E_{st} = 5$ mV and two values of the square wave amplitude. The values of E_{SW} (in mV) are: 40 (black lines and symbols) and 60 (red lines and symbols).

References

1. M. Fujuhira, J. F. Rusling, I. Rubinstein, I. (editors), Encyclopledia of Electrochemistry, Vol. 10: Modified electrodes (A. J. Bard, M. Stratmann M., editors), Wiley-VCH, 2007, Weinheim.

2. J. J. Gooding, S. Ciampi, S. The molecular level modification of surfaces: from self-assembled monolayers to complex molecular assemblies, Chem. Soc. Rev. 40 (2011) 2704-2718, doi: 10.1039/C0CS00139B.

3. R. D. Milton, T. Wang, K. L. Knoche, S. D. Minteer, Tailoring biointerfaces for electrocatalysis, Langmuir, 32 (2016) 2291-2301, doi: 10.1021/acs.langmuir.5b04742.

4. C. Cao, Y. Zhang, C. Jian, M. Qi, G. Liu, G, Advances on Aryldiazonium Salt Chemistry Based Interfacial Fabrication for Sensing Applications, ACS Appl. Mat. Interfaces 9 (2017) 5031-5049, doi: 10.1021/acsami.6b16108.

5. L. Zhang, Y. B. Vogel, B. B. Noble, V. Gonçalves, N. Darwish, A. Le Brun, J. J. Gooding, G. Wallace, M. Coote, S. Ciampi, TEMPO Monolayers on Si(100) Electrodes: Electrostatic Effects by the Electrolyte and Semiconductor Space-Charge on the Electroactivity of a Persistent Radical, J. Am. Chem. Soc. 138 (2016) 9611-9619, doi: 10.1021/jacs.6b04788.

6. V. Fourmond, E. S. Wiedner, W. J. Shaw, C. Legér, J. Am. Chem. Soc., Understanding and Design of Bidirectional and Reversible Catalysts of Multielectron, Multistep Reactions, 141 (2019) 11269-11285, doi: 10.1021/jacs.9b04854

7. V. Ball, Self-assembly processes at interfaces: multiscale phenomena, Academic Press, 2017, London.

8. P-Y. Blanchard, O. Alévêque, T. Breton, E. Levillain, TEMPO mixed SAMs: electrocatalytic efficiency versus surface coverage, Langmuir, 28 (2012) 13741-13745, doi: 10.1021/la301403w.

9. S. Fukuzumi, Y-M. Lee, W. Nam, Immobilization of Molecular Catalysts for Enhanced Redox Catalysis, ChemCatChem, 10 (2018) 1686-1702, doi: 10.1002/cctc.201701786

10. R. M. Bullock, A. K. Das, A. M. Appel, Surface Immobilization of Molecular Electrocatalysts for Energy Conversion, Chem. Eur. J., 23 (2017) 7626-7641, doi: 10.1002/chem.201605066,

11. Laviron, E., Voltammetric methods for the study of adsorbed species, in Electroanalytical Chemistry, vol. 12: Bard, A. J. Editor; Marcel Dekker: New York, 1982; pp: 53-157.

12. Laviron, E.; Roullier, L. General expression of the linear potential sweep voltammogram for a surface redox reaction with interactions between the adsorbed molecules. Applications to modified electrodes. J. Electroanal. Chem. 1980, 115, 65-74, doi: 10.1016/S0022-0728(80)80496-7.

13. Nerngchamnong, N.; Thompson, D.; Cao, L.; Yuan, L.; Jian, L.; Roeme, M.; Nijuis C. A. Nonideal electrochemical behavior of ferrocenyl-alkanethiolate SAMs maps the microenvironment of the redox unit. J. Phys. Chem. C. 2015, 119, 21978-21991, doi: 10.1021/acs.jpcc.5b05137.

14. T. J. Duffin, N. Nerngchamnong, D. Thompson, C. A. Nijhuis, Direct measurement of the local field within alkyl-ferrocenyl-alkanethiolate monolayers: importance of the supramolecular and electronic structure on the voltammetric response and potential profile, Electrochim. Acta, 311(2019)92-102, doi: 10.1016/j.electacta.2019.04.041.

15. Calvente, J. J.; Andreu, R. Intermolecular interactions in electroactive thiol monolayers probed by linear scan Voltammetry. Curr. Op. Electrochem., 2017, 1, 22-26, doi: 10.1016/j.coelec.2016.12.006.

16. C. Costentin, J. M. Saveant, Molecular approach to catalysis of electrochemical reaction in porous films, Curr. Op. Electrochem., 15 (2019) 58-65, doi: 10.1016/j.coelec.2019.03.014.

17. Gonzalez, J.; Sequi, J. A. Kinetic implications of the presence of intermolecular interactions in the response of binary self-assembled electroactive monolayers, ACS Omega, 2018, 3, 1276-1292, doi: 10.1021/acsomega.7b01995.

18. A. L. Eckermann, D. J. Feld, J. A. Shaw, T. J. Meade, Electrochemistry of redox-active self-assembled monolayers, Coord. Chem. Rev., 254(2010)1769-1802, doi: 10.1016/j.ccr.2009.12.023.

19. R. G. Compton, C. E. Banks, Understanding Voltammetry, 2nd ed., Imperial College Press, London, 2010.

20. Molina, A.; Gonzalez, J. Pulse Voltammetry in Physical Electrochemistry and Electroanalysis. Theory and applications, Springer, Heidelberg, 2106.

21. S. E. Creager, T. A. Wooster, A New Way of Using ac Voltammetry To Study Redox Kinetics in Electroactive Monolayers. Anal. Chem. 70 (1998) 4257-4263, doi: 10.1021/ac980482l.

22. A. M. Bond, N. W. Duffy, S. X. Guo, J. Zhang, D. Elton, Changing the look of Voltammetry. Can FT revolutionize voltammetric techniques as it did for NMR?, Anal. Chem. 77 (2005) 186A-195A, doi: 10.1021/ac053370k.

23. H. Adamson, A. M. Bond, A. Parkin, Probing biological redox chemistry with large amplitude Fourier transformed ac voltammetry, Chem. Commun. 53(2017)9519-9533, doi: 10.1039/C7CC03870D.

24. Y. Zhang, A. N. Simonov, J. Zhang, A. M. Bond, Fourier transformed alternating current voltammetry in electromaterials research: direct visualisation of important underlying electron transfer processes, Curr. Op. Electrochem. 10(2018)72-81, doi: 10.106/j.coelec.2018.04.016.

25. G. P. Morris, R. E. Baker, K. Gillow, J. J. Davis, D. J. Gavaghan, A. M. Bond, Theoretical analysis of the relative significance of thermodynamic and kinetic dispersion in the dc and ac voltammetry of surface confined molecules, Langmuir, 31(2015)4996-5004, doi: 10.1021/la5042635.

26. Chidsey C. E. D. Free Energy and Temperature Dependence of Electron Transfer at the Metal-Electrolyte Interface. Science, 1991, 251, 919-922

27. V. Mirčeski, S. Komorsky- Lovrić, M. Lovrić, M. Square-Wave Voltammertry: Theory and Application; Scholz, F., Ed.; Springer Verlag: Heidelberg, Germany, 2007.

28. V. Mirčeski, R. Gulaboski, M. Lovrić, I. Bogeski, R. Kappl, M. Hoth, M. Square-Wave Voltammetry: A Review on the Recent Progres. Electroanal. 2013, 25, 2411-2422

29. S. Komorsky- Lovrić, M. Lovrić, Square-wave voltammetry of quasi-reversible surface redox reactions, J. Electroanal. Chem., 384 (1995) 115-122, doi: 10.1016/0022-0728(94)03742-L.

30. J. G. Osteryoung, R. A. Osteryoung, Square Wave Voltammetry, Anal. Chem., 557 (198) 1101-110, doi: 10.1021/ac00279a004.

31. M. A. Mann, L. A. Bottomley, Cyclic Square Wave voltammetry of surface-confined quasireversible electron transfer reactions, Langmuir 31(2015)9511-9520.

32. Gonzalez, J.; Molina, A.; Abenza, N.; Serna, C.; Moreno, M. M. Square wave voltcoulometry: a new tool for the study of strongly adsorbed redox molecules. Anal. Chem. 2007, 79, 7580-7587

33. G. C. Baker, J. L. Jenkins, Square Wave Polarography, Analyst 77(1952)685-696, doi: 10.1039/AN9527700685.

34. R. Gulaboski, M. Janeva, V. Maksimova, New Aspects of Protein-film Voltammetry of Redox Enzymes Coupled to Follow-up Reversible Chemical Reaction in Square-wave Voltammetry, Electroanal. 31 (2019) 946-956, doi: 10.1002/elan.201900028.

35. R. Gulaboski, L. Mihajlov, Catalytic mechanism in successive two-step protein-film voltammetry. Theoretical study in square-wave voltammetry, Biophys. Chem. 155 (2011) 1-9, doi: 10.1016/j.bpc.2011.01.010.

36. M. Lovrić, S. Komorsky- Lovrić, Square-Wave Voltammetry of an adsorbed reactant, J. Electroanal. Chem., 248 (1988) 239-253, doi: 10.1016/0022-0728(88)85089-7.

37. R. Gulaboski, Theoretical contribution towards understanding specifi behaviour of “simple” protein-film reactions in Square-Wave Voltammetry, Electroanal. 31(2019)545-555, doi: 10.1002/elan.201800739.

38. R. Gulaboski, V. Mirceski, M. Lovric, Square-Wave protein-film voltammetry: new insights in the enzymatic electrode processes coupled with chemical reactions, J. Sol. Stat. Electrochem., 23(2019)2493-2506, doi: 10.1007/s10008-019-04320-7.

39. V. Mirčeski, E. Laborda, D. Guziejewski, R. G. Compton, New approach to electrode kinetic measurements in square-wave voltammetry: Amplitude-based quasireversible maximum, Anal. Chem., 85 (2013) 5586-5594, doi: 10.1021/ac4008573.

40. D. Bizzotto, I. J. Burguess, T. Doneux, T. Sagara, H-Z. Yu, Beyond Simple Cartoons: Challenges in Characterizing Electrochemical Biosensor Interfaces, ACS Sensors 3(2018)5-12 doi: 10.1021/acssensors.7b00840.

41. E. Laviron, L. Roullier, L. General expression of the linear potential sweep voltammogram for a surface redox reaction with interactions between the adsorbed molecules. Applications to

modified electrodes, J. Electroanal. Chem. 115(1980), 65-74, doi: 10.1016/S0022-0728(80)80496-7.

42. Mirčeski, V.; Lovrić, M.; Gulaboski, R. Theoretical and experimental study of the surface redox reaction involving interactions between the adsorbed particles under conditions of square wave Voltammetry, J. Electroanal. Chem. 2001, 515, 91-100.

43. J. Gonzalez, J. A. Sequí, Square Wave Voltcoulommetry Analysis of the Influence of the Electrostatic Environment on the Electrochemical Functionality of Redox Monolayers, ChemElectroChem 6(2019)2290-2301, doi: 10.1002/celc.201900352.

44. F. E. A. Catunda, M. F. de Araujo, A. M. Granero, F. J. Arévalo, M. G. de Carbalho, M. A. Zón, H. Fernández, Electrochim. Acta, 56(2011)9707-9713

45. Henstridge M. C.; Laborda, E.; Rees, N. V.; Compton, R. G. Marcus-Hush-Chidsey theory of electron transfer applied to voltammetry: A review. *Electrochim. Acta* 2012, *84*,12-20

46. Laborda, E.; Henstridge, M.: Batchelor-McAuley, C.; Compton, R. G. Asymmetric Marcus-Hush theory for Voltammetry, *Chem. Soc. Rev*. **2013**, *42*, 4894-4905.

Highlights

- Analysis of the influence of intermolecular interactions on the Square Wave Voltammetry (SWV) response of surface confined electroactive probes under finite kinetics conditions, is presented.
- Significant deviations in the current (degree of symmetry, location of the Quasi-Reversible Maximum) are theoretically predicted and experimentally confirmed.
- A quantitative method for obtaining kinetic and interaction parameters of the redox probes is presented and applied to mixed ferrocenylundecanethiol / decanethiol monolayers on gold electrodes at an ethanolic medium.
- An accurate and reliable estimation has been done for the kinetic rate constant for ferrocenylundecanethiol probes under conditions of strong influence of intermolecular interactions.

Graphical abstract